

Research Article

<https://doi.org/10.1631/jzus.A2300159>

Evolution mechanism and quantitative characterization of initial micro-cracks in marble under triaxial compression

Zhiliang WANG¹✉, Songyu LI¹, Jianguo WANG², Ao LI¹, Weixiang WANG¹, Chenchen FENG¹, Jingjing FU¹

¹School of Civil and Hydraulic Engineering, Hefei University of Technology, Hefei 230009, China

²School of Mechanics and Civil Engineering, China University of Mining and Technology, Xuzhou 221116, China

Abstract: The initial micro-cracks affect the evolution characteristics of macroscopic deformation and failure of rock but are often ignored in theoretical calculation, numerical simulation and mechanical experiments. In this paper, we propose a quantitative analysis model to investigate the effects of initial micro-cracks on the evolution of rock deformation and failure. The relationship between micro-crack propagation and sample failure characteristics was comprehensively studied by combining theoretical analysis with a micro-CT scanning technique. We found that with increasing confining pressure, the matrix elastic modulus of marble first increased and then tended to be stable, while the micro-cracks increased exponentially. The sensitivity ranges of the sample matrix elastic modulus and micro-cracks to confining pressure were 0-30 MPa and 30-50 MPa, respectively. The porosity and Poisson's ratio decreased exponentially. The increasing proportion of internal micro-cracks led to an increase in sample non-uniformity. The rock samples presented mainly shear failure under triaxial compression, and the failure angle decreased linearly with increasing confining pressure. The convergence direction of cracks decreased gradually. This quantitative analysis model could accurately portray the relationship between the overall macroscopic deformation and the deviatoric stress of samples at the compaction stage and the linear elastic stage. It is a useful tool to characterize rock stress-strain behaviors and for geological disaster prevention.

Key words: Rock materials; Initial micro-cracks; Triaxial compression; Constitutive relationship; Crack evolution


1 Introduction

As the shallow mineral geological resources around the world are on the verge of exhaustion, the depth of underground mining is increasing year by year (Xie, 2019) and mining conditions are becoming increasingly complex (Chen, 2017). Due to the compound effects of geological conditions (such as tectonic stress, plate and shell movement) and human activities (such as the disturbance of shield excavation and blasting mining vibration) (Li et al., 2015; Xu et al., 2022; Liu et al., 2019) numerous micro-cracks become randomly distributed in the

underground engineering rock mass (Liu and Dai, 2021). Micro-cracks can cause difficulties in deep geotechnical engineering support and frequent geological disasters (Li et al., 2017a), including roof collapse, rockburst and coal (gas) outbursts as a result of unstable deformation of the rock mass structure (Zhang and Zhao, 2014). Such disasters can be regarded as the result of the generation and propagation of rock cracks (Saadat and Taheri, 2019; Dehestani et al., 2022; Wu et al., 2017). Therefore, the accurate characterization of mechanical properties and crack evolution in rocks under different loading conditions is of great significance for evaluating the structural stability of deep underground engineering and providing early warning of related geological hazards.

The rock mass is an important component of an underground engineering structure. It is a natural heterogeneous material that includes the rock matrix and micro-cracks (pores) (Nur, 1971; Pakzad et al., 2023; Zhou et al., 2014; Zhou et al., 2019b; Morgan et

✉ Zhiliang WANG, cvewzL@hfut.edu.cn

 Zhiliang WANG, <https://orcid.org/0000-0001-9989-3109>

Songyu LI, <https://orcid.org/0000-0002-8884-3226>

Received Mar. 26, 2023; Revision accepted Apr. 23, 2023;
Crosschecked

al., 2013; Eberhardt et al., 1998). The random distribution of micro-cracks in the rock matrix determines the internal structural characteristics of the rock and affects its physical and mechanical properties (Cao et al., 2015; Daniel et al., 2023; Bahrani and Kaiser, 2017). Zuo et al. (2019) studied the growth of cracks in rocks under different confining pressures and temperatures. They derived a crack growth model for triaxial compression and verified their model with experimental results. Their results showed that their model could describe the nonlinear crack growth behaviors of rock under triaxial compression. Zhang et al. (2020) abstracted brittle rock materials into skeletons and cracks, and established a constitutive model to consider the initial pore closure effect with instantaneous strain and statistical damage theory. This constitutive model for brittle rocks could describe the relationships among the mechanical properties of pre-peak macroscopic deformation of brittle rock, initial pores and external confining pressure. Li and Wong (2012) adopted finite element method (FEM) and non-linear dynamics method to investigate the effects of the pre-existing flaw inclination angle on the cracking processes. They found that the crack initiation sequences, resultant crack types and the overall crack pattern all changed with loading conditions. Tensile cracks occurred before shear cracks when the sample was subjected to a low loading rate or low confining pressure.

The damage evolution and failure characteristics of a sample under compression are also affected by its crack evolution (Mavko and Nur, 1978; Shreedharan and Kulatilake, 2016; David et al., 2012; Johnson and Rasolofosaon, 1996; Rosengren and Jaeger, 1968; Zhou et al., 2018). Peng et al. (2016) pointed out that the proportion of initial micro-cracks in rocks could be regarded as initial micro-crack damage. The existence of initial micro-cracks increased the heterogeneity and significantly reduced the elastic modulus and peak strength of the rock. Li et al. (2017b) obtained stress-strain curves of coal, shale and tight sandstone through uniaxial compression tests and established micro-damage constitutive models for those rocks based on power function, Weibull and Gaussian distributions of cracks. Their results showed that these new micro-damage constitutive models could accurately represent the pre-peak stress-strain relationship of coal, shale and tight sandstone. Zhao

and Liu (2012) used Hooke's law based on natural strain and engineering strain to describe the deformation of internal pores and other parts of porous rock, respectively. They established a three-dimensional stress-strain relationship to represent the composite characteristics of anisotropic cracks and the elastic matrix in rock materials. The proportion of initial micro-cracks in different rock materials varied and was an important parameter to describe the initial macroscopic deformation and the stress-strain shape of a sample. The above experimental studies showed that the initial macroscopic deformation (typical nonlinear mechanical deformation) of a sample under compression was closely related to the initial micro-cracks.

The stress-strain relationship is fundamental for the stress and deformation analysis of rocks (including micro-cracks and pores) (Chang and Lee, 2004) and has been studied under various loadings and environments. Zhang et al. (2021) explored the stress-strain characteristics and energy evolution mechanism of coal containing gas under different stress and gas conditions using a thermo-fluid-solid coupling triaxial servo seepage test device. They proposed a damage constitutive model of coal based on a heterogeneous Weibull function, energy dissipation function and plastic strain function. Bieniawski (1967) summarized the stage of sample stress-strain curves through rock mechanics experiments. The stage could be roughly represented by internal crack closure, crack initiation and crack propagation. He pointed out that different occurrence states of micro-cracks in a sample corresponded to different characteristic stresses. The end of the crack closure stage was marked by crack closure stress, the end of the elastic deformation stage by crack initiation stress, and the crack propagation stage by damage stress and peak stress. Based on the phase analysis of stress-strain curves, Martin (1997) proposed the definition and corresponding calculation method for micro-crack strain as a quantitative description of the evolution of stress and crack strain in the compression process of a sample. He also developed a procedure to determine the crack closure stress and crack initiation stress based on the stress micro-crack volumetric strain curve. Zhao et al. (2017) studied the nonlinear rheological mechanical properties of hard rock through a cyclic recursive incremental unloading experiment. They successfully separated viscoelastic strain from viscoplastic strain in the total creep curve

with a newly proposed data processing algorithm. They studied the elasto-viscoplastic rheological behaviors of lithic rocks under triaxial compression and established a nonlinear elasto-viscoplastic rheological model which includes various deformation components (Hooke body, parallel combination of Hooke and plastic sliding body, Kelvin body and generalized Bingham body). In this study, we analyzed the reasons for tolerance fluctuations, constructed the condition-driven adaptive design method for tolerance by using the hidden Markov model algorithm, and then presented the results of some experiments on the precision stamping process and discussed the feasibility and effectiveness of the adaptive design method.

The above studies have analyzed the stress-strain relationship of rock in the pre-peak stage, but have rarely quantitatively analyzed the proportion of initial micro-cracks and the evolution of mechanical characteristics with confining pressure. The relationship between crack growth and the macroscopic failure characteristics of samples under triaxial compression has also not been fully discussed. Therefore, a quantitative analysis model is necessary to consider the initial crack (pores) closure effect of rocks. In this study, a theoretical model for the quantitative analysis of the initial proportion of micro-cracks of rock was first established based on

the stress decomposition of triaxial compression. Then, the fitting interval for the accurate analysis of initial rock micro-cracks was determined through the stage analysis of stress-strain curves. The model was verified against experimental data. Finally, the fracture evolution characteristics of the loaded rock samples were analyzed with CT scanning. The results provide reference parameters for numerical simulation when the initial microcracks in the rock and matrix are modeled separately.

2 Model establishment

Dynamic and static tests on rock showed that its mechanical properties of deformation and failure were closely related to micro-crack propagation (closure, initiation, extension and interpenetration) in the rock. The increasing slope of the stress-strain curve also changes gradually with the growth of micro-cracks. The pre-peak stage of the stress-strain curve can be roughly divided into three stages (Corkum and Martin, 2007), based on the slope change (Fig. 1), where σ_{cc} and σ_{ci} are the end of compaction point stress and crack initiation stress, respectively, and can be identified by theoretical calculation or monitoring means (such as acoustic emission). σ_p is the peak stress.

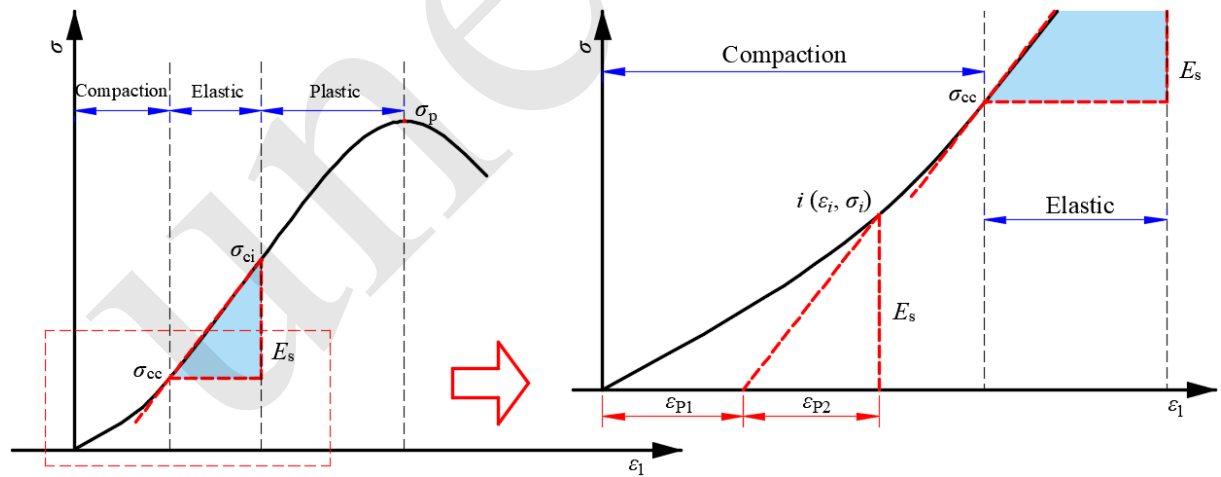


Fig. 1 Deformation stage of pre-peak stress-strain curves of rock

The stress-strain relationship in the compaction stage (the concave growth stage of the stress-strain curve) is closely related to the volume of initial micro-cracks. When a sample is loaded to the crack closure stress, the initial micro-cracks inside the

sample are basically closed, and the slope of the stress-strain curve does not change (the linear elastic stage). The slope of the corresponding position curve is the elastic modulus E_s of the sample, and the average ratio of the circumferential strain to the axial

strain at the corresponding stage is the Poisson's ratio μ_s . Therefore, the initial micro-cracks can be quantitatively characterized by the stress-strain relationship during the compaction and the linear elastic stages.

Natural rock can be regarded as a composite rock with a matrix and micro-cracks (pores). The contribution of micro-crack deformation to the overall macroscopic deformation of rock can be analyzed using effective medium theory (Cai et al., 2017). As shown in Fig. 1, the strain ε of rock at the compaction stage and elastic stage has two components: the partial strain ε_{p1} of the matrix and the partial strain ε_{p2} of the cracks:

$$\varepsilon = \varepsilon_{p1} + \varepsilon_{p2} \quad (1)$$

Introducing the proportion of initial micro-cracks in the rock, the axial partial strain of the matrix and cracks is given by

$$\varepsilon_{p1} = (1 - \frac{V_c}{V})\varepsilon_{mz} \quad (2)$$

$$\varepsilon_{p2} = \frac{V_c}{V}\varepsilon_{cz} \quad (3)$$

where V_c is the initial micro-crack volume in the

sample, V is the overall volume of the sample, ε_{mz} is the axial strain of the matrix, and ε_{cz} is the axial strain of the micro-cracks.

The overall macroscopic strain of the sample is the summation of the two components:

$$\varepsilon = (1 - \frac{V_c}{V})\varepsilon_{mz} + \frac{V_c}{V}\varepsilon_{cz} \quad (4)$$

The slope variation of the stress-strain curve of rock samples at the compaction stage and the linear elastic stage shows that when the sample is loaded to the crack closure stress, the micro-cracks inside the sample are basically closed, and the stress-strain relationship is approximately linear and follows the generalized Hooke's law as

$$\varepsilon_{mz} = \frac{1}{E_m}[\sigma_z - \mu_m(\sigma_x + \sigma_y)] \quad (5)$$

where E_m is the elastic modulus and μ_m Poisson's ratio of the rock matrix. σ_x , σ_y and σ_z are the principal stresses.

The sampling process and corresponding representative volume element (RVE) are shown in Fig. 2.

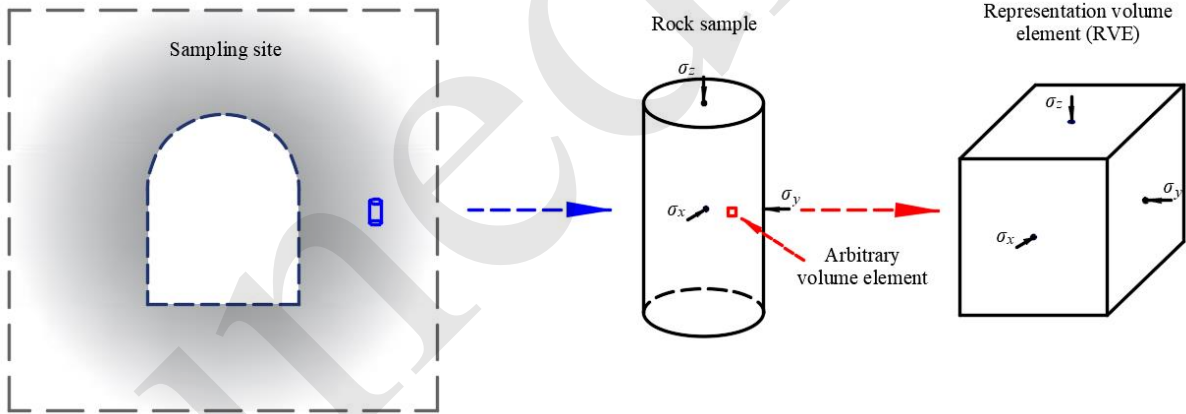


Fig.2 Sampling process of rock sample and corresponding representative volume element

First, the stress environment at the sampling site should be considered in the mechanical test and the result analysis of the rock sample. Then, the rock sample is assumed to be an aggregate (n equal parts), and one micro-element (the arbitrary volume element) is taken for analysis. A representative volume element (Fig. 3) is taken to characterize the deformation characteristics of rock under external load.

The axial strain of the micro-element after loading can be expressed as

$$d\varepsilon_{cz} = \frac{z - z_0}{z} \quad (6)$$

where z and z_0 are the equivalent micro-crack lengths before and after loading, respectively.

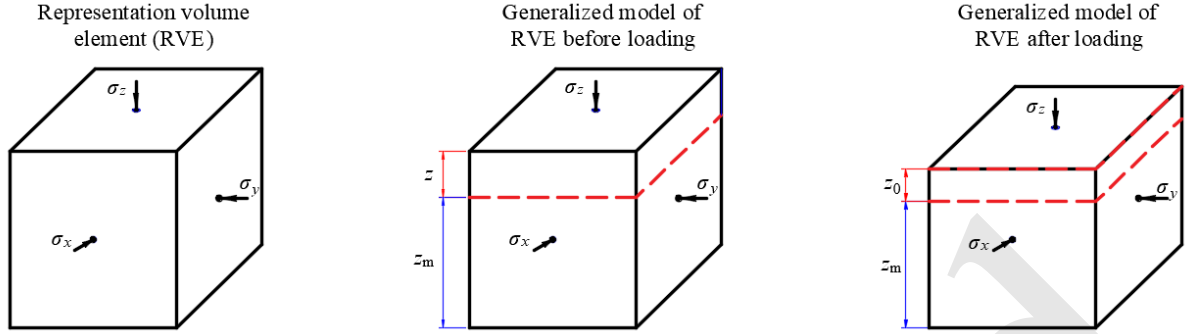


Fig.3 Conception and deformation of a representation volume element in the sample

The deformation of the micro-cracks inside rock is different from that of the matrix. The micro-cracks in natural rocks are randomly distributed in the matrix. At present, it is technically unrealistic to measure the strain field borne by micro-cracks (Tang et al., 2019). In addition, the cyclic loading and unloading test results of rock show that the unloading curves do not return along the original loading path but form a hysteretic ring. The existence of micro-cracks makes rock neither completely elastomeric nor completely plastomeric (Zhang et al., 2022). Therefore, the equivalent micro-crack has the plastic deformation characteristic of incomplete recovery. Natural strain can describe this part of deformation more accurately (Freed, 1995). Combined with the above analysis, the deformation of an equivalent micro-crack unit is described by natural strain as

$$d\varepsilon_{cz} = \int_z^{z_0} -\frac{dz}{z} = -\ln \frac{z_0}{z} \quad (7)$$

Combining Eqs. (6) and (7) gives

$$\frac{z_0}{z} = e^{-d\varepsilon_{cz}} \quad (8)$$

In the RVE, the deformation of micro-cracks is assumed to follow the generalized Hooke's law (Xie et al., 2022) as

$$d\varepsilon_{cz} = \frac{1}{E_c} [d\sigma_z - \mu_c (d\sigma_x + d\sigma_y)] \quad (9)$$

where E_c is the elastic modulus and μ_c the Poisson's ratio of the rock micro-cracks.

Therefore, the strain increment is obtained based on Eqs. (6), (8) and (9) as

$$d\varepsilon_{cz} = 1 - e^{-\frac{1}{E_c} [d\sigma_z - \mu_c (d\sigma_x + d\sigma_y)]} \quad (10)$$

The strain of the internal initial micro-cracks is then expressed as

$$\varepsilon_{p2} = \int_{i=1}^n d\varepsilon_{cz} \quad (11)$$

Or

$$\begin{aligned} \varepsilon_{p2} &= \int_{i=1}^n \frac{V_c}{nV_0} (1 - e^{-\frac{1}{E_c} [d\sigma_z - \mu_c (d\sigma_x + d\sigma_y)]}) \\ &= \frac{V_c}{V} (1 - e^{-\frac{1}{E_c} [\sigma_z - \mu_c (\sigma_x + \sigma_y)]}) \end{aligned} \quad (12)$$

where V_0 is the volume of the RVE and V_c is the volume of the micro-cracks in the RVE.

Combining Eqs. (4), (5) and (12) obtains the quantitative analysis model of initial micro-cracks as

$$\begin{aligned} \varepsilon &= (1 - \frac{V_c}{V}) \frac{1}{E_m} [\sigma_z - \mu_m (\sigma_x + \sigma_y)] \\ &+ \frac{V_c}{V} (1 - e^{-\frac{1}{E_c} [\sigma_z - \mu_c (\sigma_x + \sigma_y)]}) \end{aligned} \quad (13)$$

Each parameter in this equation has clear physical significance but is difficult to measure directly using conventional rock mechanics methods and experiments. They can be calculated indirectly through the stress-strain relationship of the rock under triaxial compression.

In the conventional triaxial compression test ($\sigma_3 = \sigma_x = \sigma_y$), the test process is first to increase the confining pressure to a preset value, and then apply the axial stress. At this time, the stress applied to the sample is the deviatoric stress ($\sigma_x - \sigma_y$). That is, the experimental results monitored by the triaxial compression device measure the relationship between the deviatoric stress and the sample strain (axial and circumferential). Through stress decomposition, the stress state of the triaxial compression sample can be decomposed into the compound action of hydrostatic pressure and deviatoric stress (Fig. 4). The uniaxial compression is a special case of triaxial compression ($\sigma_x = \sigma_y = 0$ MPa).

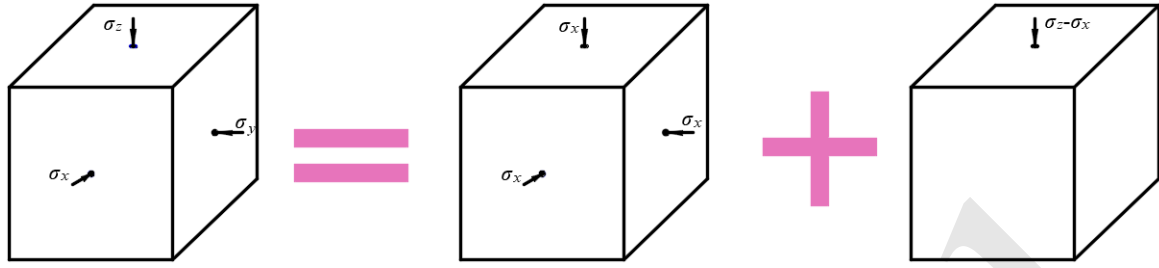


Fig. 4 Load stress decomposition of conventional triaxial compression samples

The above stress decomposition shows that the strain of rock obtained by a conventional triaxial compression experiment is due to deviatoric stress. Therefore, the quantitative analysis model of the initial micro-cracks inside the sample can be expressed as

$$\varepsilon_T = (1 - \frac{V_c}{V}) \frac{1}{E_m} (\sigma_z - \sigma_x) + \frac{V_c}{V} (1 - e^{-\frac{\sigma_z - \sigma_x}{E_c}}) \quad (14)$$

where ε_T is the axial strain of the sample under triaxial compression.

3 Results

3.1 Model validation

To verify this proposed model, a series of triaxial tests ($\sigma_3=0-50$ MPa) were carried out on the RTX-4000 triaxial electro-hydraulic servo loading

system at the China University of Mining and Technology (Fig. 5). The marble used in the test was taken from Sichuan Province, China (Jinping II Hydropower Station), and the average principal stress at the sampling site was between 35 and 50 MPa. XRD test results showed the mineral composition of the marble material was mainly dolomite (69.31%), calcite (20.35%) and quartz (5.44%). Each marble sample was taken from the same rock block and processed into a standard cylinder, 50 mm in diameter \times 100 mm high. The sample was polished according to the recommendations of the ISRM (International Society of Rock Mechanics) until it met the test requirements (e.g., end face parallelism less than ± 0.05 mm) (Fairhurst and Hudson, 1999). A photo of marble samples is shown in Fig. 5.

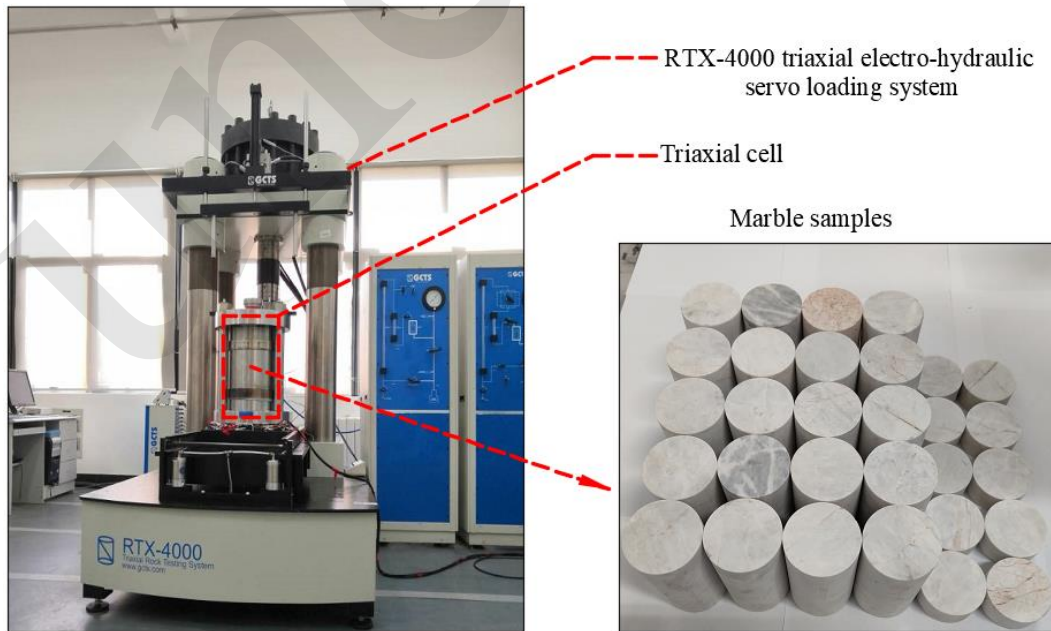


Fig. 5 Photos of triaxial compression device and marble samples

Before the triaxial compression experiment, the longitudinal wave velocity and density were measured for each sample. Based on the measurement results, the samples differing greatly from the average were discarded to eliminate the discreteness among the samples as far as possible. Among the samples in the triaxial compression test, the average wave velocity was 3700 m/s and the average density 2800 kg/m³. The detailed steps of the triaxial com-

pression test and corresponding control conditions (confining pressure loading rate and axial pressure loading rate) are given in reference (Wang et al., 2022). The deviatoric stress axial strain curve of a triaxial compression marble sample is shown in Fig. 6. The deviatoric stress at each segment point is equal to the corresponding axial stress minus the confining pressure (e.g., $\sigma_{ccd} = \sigma_{cc} - \sigma_3$).

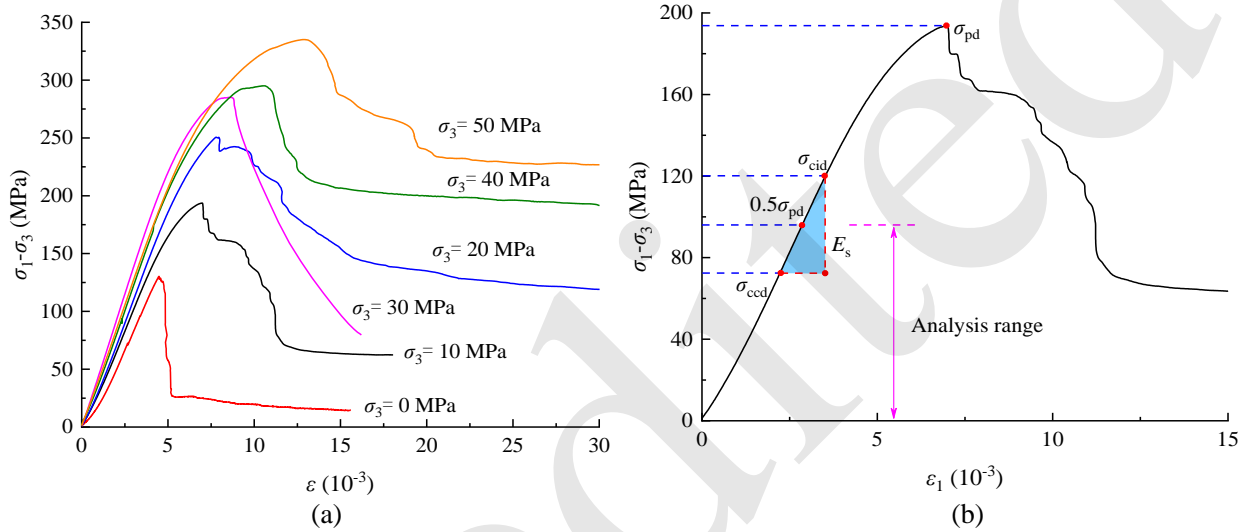


Fig. 6 Stress-axial strain curve of triaxial compression marble samples and analysis range of the model:
(a) Stress-axial strain curve; (b) Analysis range of the mode

The above analysis showed that the initial micro-cracks of the sample can be quantitatively characterized through the compaction stage and the linear elastic stage of the stress-strain curve. Therefore, it was necessary to quantitatively determine the segment points of the linear elastic stage. Comparative analysis was conducted on the stress distribution at characteristic points (e.g., σ_{ccd}) of the marble triaxial compression samples in this study. Combined with the acoustic emission monitoring results of crack initiation points in the literature (Zhou et al., 2019a), we found that half of the peak deviatoric stress ($0.5\sigma_{pd}$) of the triaxial compression samples is a definite position point, which is also located in the elastic stage of samples. That is, half of the peak deviatoric stress is lower than the stress at the crack initiation point of the sample. Therefore, the analysis range of the above quantitative analysis model for

initial micro-cracks of samples was $[0, 0.5\sigma_{pd}]$, i.e., from the initial loading point to half of the peak deviatoric stress (Fig. 6b).

Based on the newly established quantitative analysis model, the stress-strain curves of each marble sample under triaxial compression and their corresponding fittings are shown in Fig. 7. Under each confining pressure, the results from the micro-cracks quantitative analysis model closely matched the test results (goodness of fit R^2 all greater than 0.999). The above results indicate that the quantitative analysis model proposed in this paper can accurately characterize the relationship between the overall macroscopic deformation and the deviatoric stress in the compaction stage (and the linear elastic stage) under triaxial compression. The fitting equations are as follows:

$$\sigma_3 = 0 \text{ MPa} \quad \varepsilon = (1 - 9.10 \times 10^{-4}) \frac{\sigma}{36817.90} + 9.10 \times 10^{-4} (1 - e^{-\frac{\sigma}{22.81}}) \quad (14)$$

$$\sigma_3 = 0 \text{ MPa} \quad \varepsilon = (1 - 9.10 \times 10^{-4}) \frac{\sigma}{36817.90} + 9.10 \times 10^{-4} (1 - e^{-\frac{\sigma}{22.81}}) \quad (15)$$

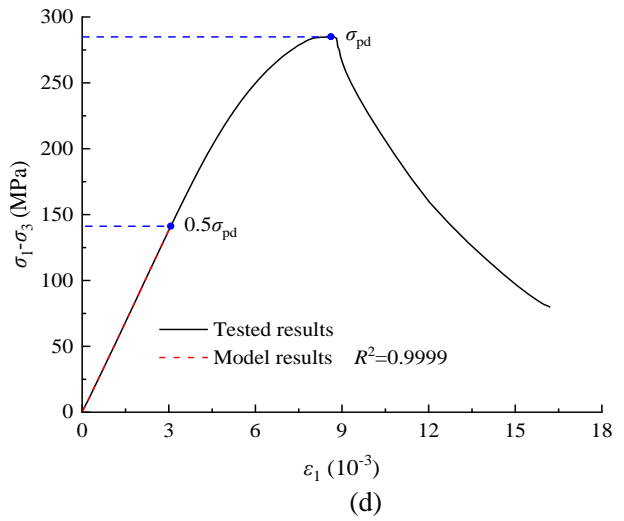
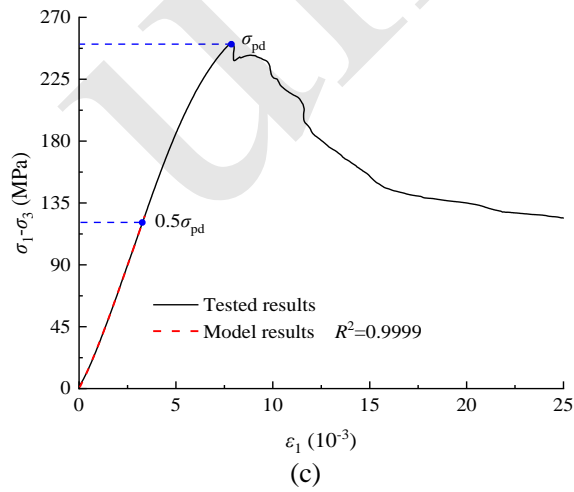
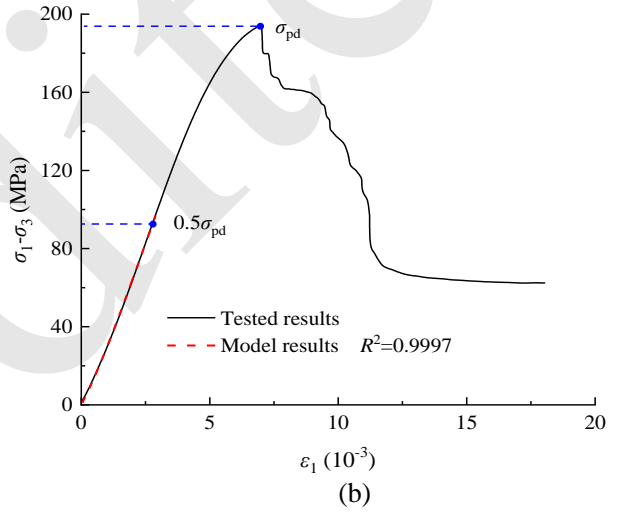
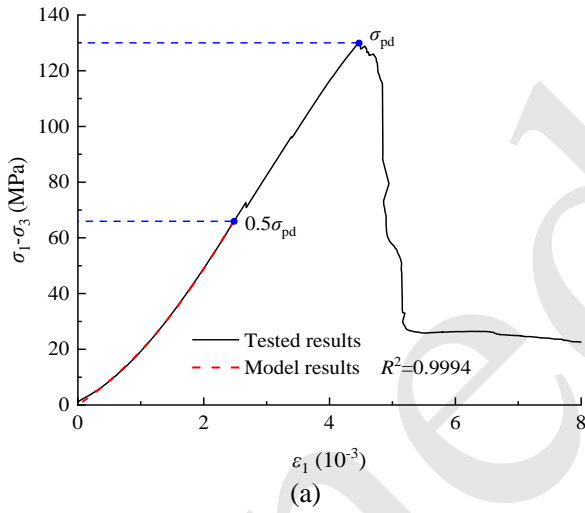
$$\sigma_3 = 10 \text{ MPa} \quad \varepsilon = (1 - 2.79 \times 10^{-4}) \frac{\sigma}{37029.14} + 2.79 \times 10^{-4} (1 - e^{-\frac{\sigma}{22.85}}) \quad (16)$$

$$\sigma_3 = 20 \text{ MPa} \quad \varepsilon = (1 - 3.34 \times 10^{-4}) \frac{\sigma}{41081.38} + 3.34 \times 10^{-4} (1 - e^{-\frac{\sigma}{28.48}}) \quad (17)$$

$$\sigma_3 = 30 \text{ MPa} \quad \varepsilon = (1 - 3.55 \times 10^{-5}) \frac{\sigma}{44940.03} + 3.55 \times 10^{-5} (1 - e^{-\frac{\sigma}{29.13}}) \quad (18)$$

$$\sigma_3 = 40 \text{ MPa} \quad \varepsilon = (1 - 1.85 \times 10^{-4}) \frac{\sigma}{43163.70} + 1.85 \times 10^{-4} (1 - e^{-\frac{\sigma}{38.95}}) \quad (19)$$

$$\sigma_3 = 50 \text{ MPa} \quad \varepsilon = (1 - 6.96 \times 10^{-5}) \frac{\sigma}{43110.75} + 6.96 \times 10^{-5} (1 - e^{-\frac{\sigma}{54.89}}) \quad (20)$$



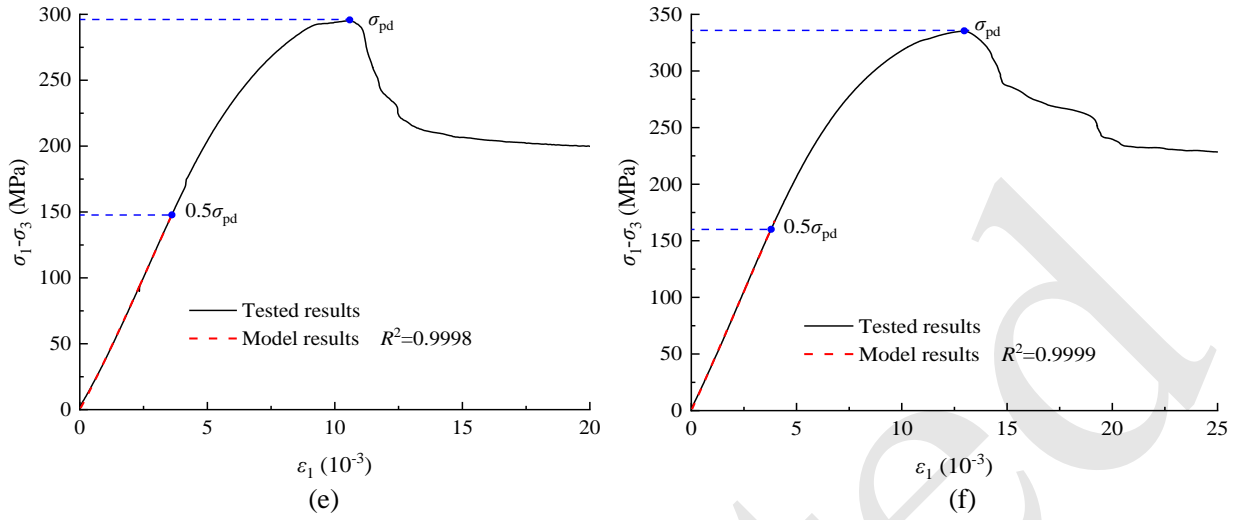


Fig. 7 Comparison between the quantitative crack analysis model curve and marble test results: (a) $\sigma_3=0$ MPa; (b) $\sigma_3=10$ MPa; (c) $\sigma_3=20$ MPa; (d) $\sigma_3=30$ MPa; (e) $\sigma_3=40$ MPa; (f) $\sigma_3=50$ MPa

3.2 Variation of model parameters with confining pressure

The above experimental results show that the initial nonlinear effect gradually decreases with the increase of confining pressure (Fig. 6a). Moreover, the initial stress-strain curves are very close under high confining pressure. This indicates that the confining pressure has a great influence on the degree of closure of the initial micro-cracks in the samples. The

parameters for elastic matrix and crack deformation of the marble samples under triaxial compression are shown in Table 1, where μ_s is the Poisson's ratio and E_s the elastic modulus (the calculation method is from reference (Taheri et al., 2020)). E_c and E_m are the elastic modulus of the cracks and matrix, respectively. E_m is equivalent to the elastic modulus (E_s) of the sample.

Table 1 Variation of deformation parameters for rock matrix and crack with confining pressure

σ_3 (MPa)	V_C/V	E_c (MPa)	E_m (GPa)	E_s (GPa)	μ_s
0	9.10×10^{-4}	22.81	36.82	33.33	0.34
10	2.79×10^{-4}	22.85	37.03	36.87	0.19
20	3.34×10^{-4}	28.48	41.08	40.18	0.15
30	3.55×10^{-5}	29.13	44.94	46.18	0.17
40	1.85×10^{-4}	38.95	43.16	42.33	0.17
50	6.96×10^{-5}	54.89	43.11	42.91	0.14

Table 1 shows that the elastic modulus of micro-cracks under each confining pressure was numerically three orders of magnitude different from that of the matrix. This verifies the rationality of using

natural strain to describe the micro-crack deformation in the derivation of the above quantitative crack analysis model. Fig. 8 shows the relationship between the elastic modulus of the samples (calculated in ref-

erence (Taheri et al., 2020)), the elastic modulus of the matrix (calculated using the model in this paper) and the elastic modulus of the micro-cracks with confining pressure. Fig. 8a and Table 1 show that the elastic modulus of the matrix E_m was 33.33 GPa and that of the sample E_s was 36.82 GPa under uniaxial compression ($\sigma_3=0$ MPa) – a difference of about 10%. For the samples under triaxial compression ($\sigma_3=10$ -50 MPa), the difference between E_m and E_s was less than 3%. The above results indicate that the elastic mod-

ulus of the samples was basically the same as that of the matrix, which verifies the correctness of the quantitative crack analysis model. It also shows that our proposed model can be used to calculate the elastic modulus of samples. With σ_3 increasing from 0 to 50 MPa, the E_m and E_s of the sample increased at first ($\sigma_3=0$ -30 MPa) and then tended to be stable ($\sigma_3=30$ -50 MPa). The elastic modulus of the sample matrix was sensitive to σ_3 in the range of 0 to 30 MPa.

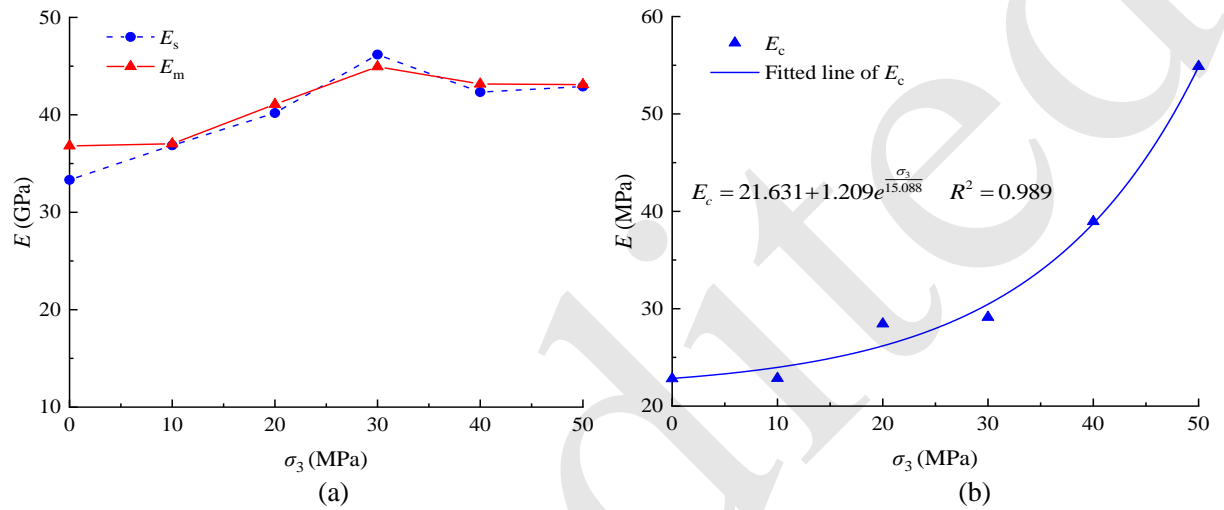


Fig. 8 Influence of confining pressure on sample modulus parameters: (a) Sample elastic modulus and matrix elastic modulus; (b) Cracks elastic modulus

Fig. 8b shows the relationship between the elastic modulus of the sample micro-cracks E_c and confining pressure. The results show that with increasing σ_3 , the elastic modulus of the micro-cracks of the samples increases exponentially. The fitting curve is shown in Fig. 8b. E_c increased slowly when σ_3 ranged from 0 to 30 MPa, and increased sharply when it exceeded 30 MPa. The above results demonstrate that the confining pressure condition for the closure of micro-cracks inside the sample was about 30 MPa. Combined with the results of Fig. 7a, the sensitivity range of the sample matrix elastic modulus to con-

fining pressure was 0-30 MPa, while that of the sample micro-cracks was 30-50 MPa.

Fig. 9 shows the variation of the porosity and Poisson's ratio of samples with confining pressure, and the fitting curve. Comparing Fig. 9a with Fig. 8a shows that the variation of porosity is negatively correlated with that of the matrix elastic modulus: i.e., when the porosity of the sample is high, the elastic modulus of the sample is correspondingly low. For example, the sample with a confining pressure of 30 MPa had the lowest porosity and the highest elastic modulus.

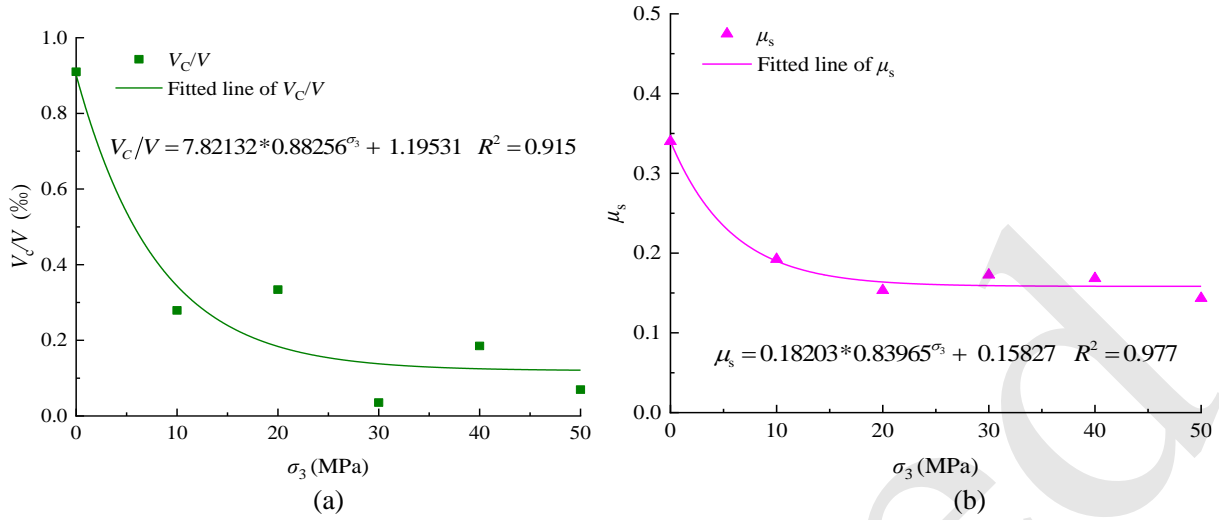


Fig. 9 Variation of porosity and Poisson's ratio of the sample with confining pressure: (a) Porosity; (b) Poisson's ratio

On the whole, an increase of σ_3 will significantly reduce the porosity and Poisson's ratio of samples. With the increase of confining pressure from 0 to 50 MPa, the porosity of the samples gradually decreased from 9.10×10^{-4} to 6.96×10^{-5} (Fig. 9a) and the Poisson's ratio from 0.34 to 0.14 (Fig. 9b). Note that the decrements of porosity and Poisson's ratio in the σ_3 range of 0-10 MPa accounted for 75% of the corresponding total decrement when σ_3 increased from 0 to 50 MPa. The existence of confining pressure has a great influence on the porosity and Poisson's ratio.

By comparing the results of Fig. 9a and 9b, the porosity and Poisson's ratio of the samples decrease gradually with increasing confining pressure in the same function. The corresponding fitting formulas are shown in Fig. 8. The above results demonstrate that the samples with high confining pressure are denser, and the circumferential and axial deformation are relatively more synchronous during compression

failure (compared with the samples under low confining pressure). The macroscopic deformation of the sample under triaxial compression is closely related to the proportion of micro-cracks inside the sample. The increase of the proportion of micro-cracks will increase the non-uniform deformation of the sample.

3.3 Failure characteristics

To explore the relationship between internal crack propagation and failure characteristics, CT scanning was performed on the samples (the confining pressure was as taken as 0 MPa, 30 MPa or 50 MPa) after the aforementioned triaxial compression experiment. A 3D reconstruction of sample failure was carried out, and sections of typical axial positions were selected to illustrate the internal failure characteristics. Typical axial section positions were taken as (diameter)=7, 14, 21, 28, 35 and 42 mm, respectively.

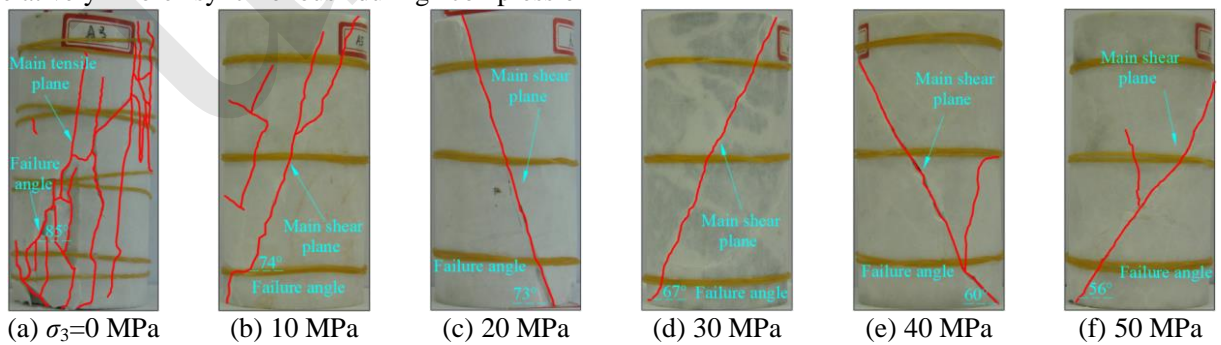


Fig. 10 Failure characteristics of triaxial compression marble samples

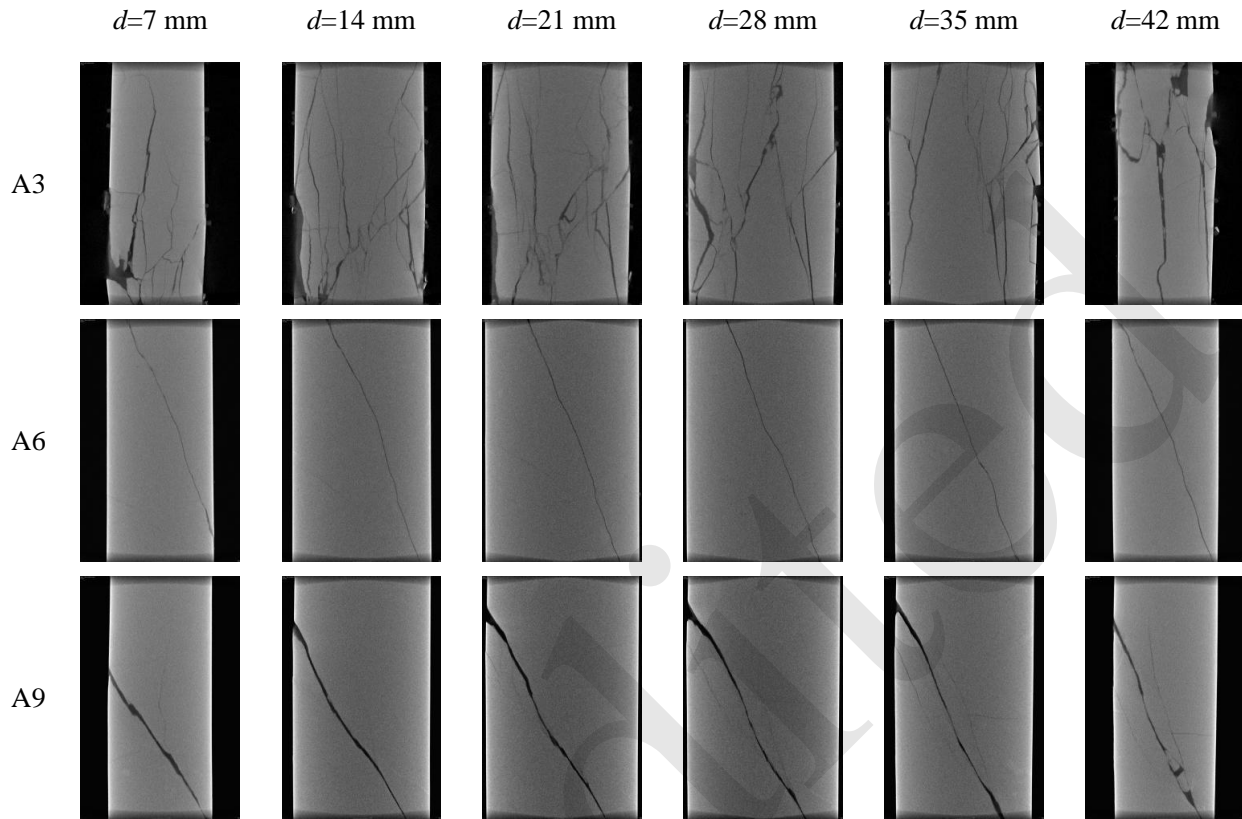


Fig. 11 CT scan sections of triaxial compression marble specimen (different axial positions)

The surface failure characteristics are shown in Fig. 10 and the CT scan sections of the samples in Fig. 11. Fig. 9a and Fig. 10 (A3) show that the sample under uniaxial compression ($\sigma_3=0$ MPa) had the most surface and internal cracks. The tensile failure is obvious. Comparison of the surface image of the damaged sample with the CT scanning results shows clearly that the CT scanning section image better reveals the propagation of the internal cracks in the sample. According to Fig. 10b-f and Fig. 11 (A6 and A9), the number of surface and internal cracks under triaxial compression ($\sigma_3=10-50$ MPa) decreased at first and then increased with confining pressure, but the number of surface and internal cracks was much lower than that under uniaxial compression. All samples under triaxial compression showed obvious shear failure. The angle (macroscopic failure angle γ) between the main macroscopic failure surface and the horizontal plane of each sample is shown in Fig. 10a-f.

4 Discussion and remarks

4.1 Crack propagation

The failure process of a sample is the propagation process of internal cracks. Combined with the above analysis of the macroscopic failure diagram (Fig. 9 and Fig. 10) of the compressed sample, the evolution of the internal mesoscopic cracks in the compression failure process is qualitatively described in Fig. 12 (Bieniawski, 1967), where σ_{dd} is the damage deviatoric stress of the sample. In addition, the damage deviatoric stress point is the turning point in dominance from compaction to dilatancy. It is also the division point from stable crack propagation to unstable crack propagation in the sample.

Natural marble samples have micro-cracks (pores) and these initial internal micro-cracks will be gradually closed in response to a continuous external load. As shown in Fig. 12, when an external load was applied to σ_{ccd} , the initial internal micro-cracks were basically closed. With the continuous load, the sample showed obvious elastic deformation characteristics. Therefore, the elastic modulus and Poisson's

ratio of the sample were calculated from the data at this stage. When the axial load was applied to σ_{cid} , new cracks began to occur inside the sample, and the

elastic deformation characteristics of the sample gradually disappeared.

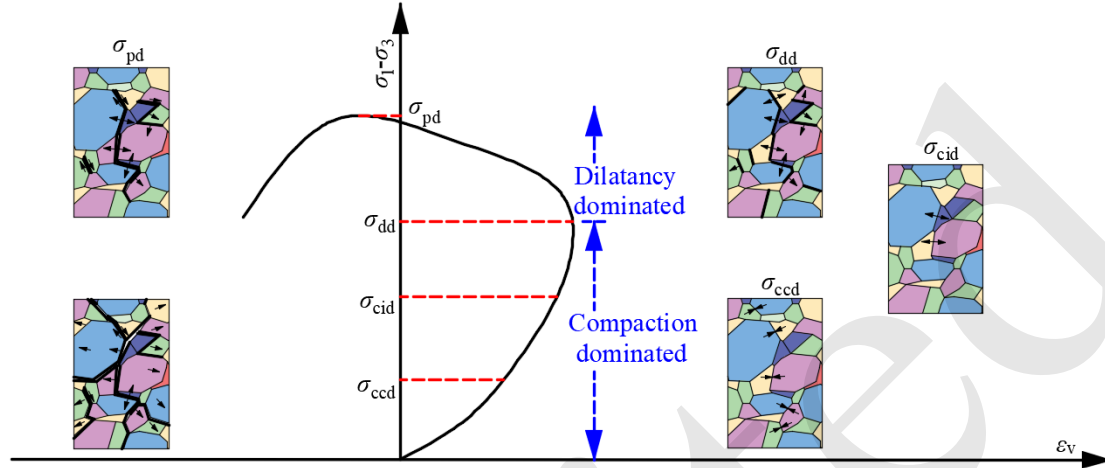


Fig. 12 Sketch of stage evolution characteristics of micro-cracks in samples

With the continuous load, the internal cracks continuously expanded (stable expansion stage), and the plastic deformation of the sample gradually appeared. When the axial load was applied to σ_{dd} , the dominant compaction phase of volumetric strain ended and the volumetric strain reached its maximum. After σ_{dd} , the volumetric strain changed to the dilatancy dominated phase, and the volumetric strain continuously decreased. At this stage, the internal cracks began to expand unsteadily and gradually coalesced to form macroscopic cracks (when the axial stress of the sample was near to σ_{pd}). After σ_{pd} , a macroscopic crack plane formed inside the sample and gradually penetrated the outer surface of the sample. From then on, the sample gradually lost its mechanical strength and eventually became unstable

and failed.

4.2 Correlation of failure characteristics and crack propagation

In the mesoscopic damage and failure analysis of the loaded rock, non-penetrating micro-cracks in rock samples are generally simplified to circular coin cracks or elliptical disk cracks and airfoil cracks in plane strain analysis (Li et al., 2023; Li et al., 2018), as shown in Fig. 13. According to the above analysis, new cracks in marble samples are initiated after the elastic stage (initiation point σ_{cid}). This is because with a continuously increasing load the crack tip strength factor becomes greater than its critical stress intensity factor, and the internal crack of the sample begins to expand.

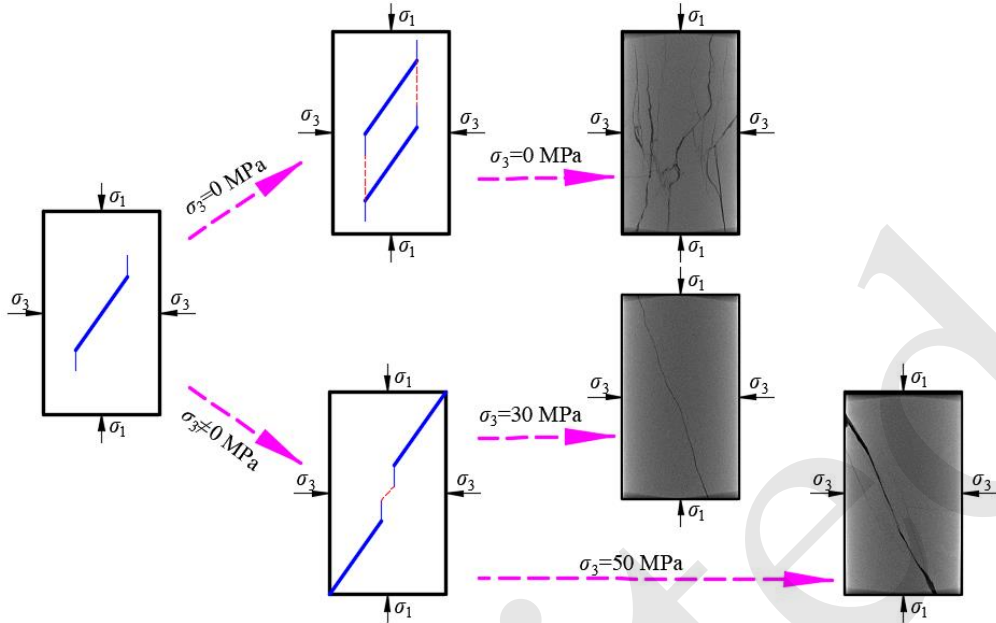


Fig. 13 Macroscopic crack propagation mode of triaxial compression sample

For the compressed sample, the initiation of internal cracks indicates only the beginning of sample damage and failure. When the internal micro-cracks coalesce with each other (the bridge connection between the cracks), the instability failure of the sample can be observed. Therefore, the propagation mode of the internal crack in the sample can be described using the connecting process of the double-crack system (Cao et al., 2016).

For marble samples under uniaxial compression, with the increase of axial strain, new tensile cracks occur at the crack tips. Due to the absence of confining pressure, the new cracks spread along the direction parallel to the axial stress, and gradually converge to form a macroscopic tensile failure surface. With the increase of load, the lateral deformation of the macroscopic tensile failure surface continuously increases. When the lateral deformation exceeds the deflection, the tensile failure surfaces will break and connect with each other, resulting in splitting tensile failure of the sample under uniaxial compression.

For a sample under triaxial compression, the confining pressure effectively inhibits the propagation process of internal micro-cracks. Only those cracks parallel to the direction of the deviatoric stress develop. With continuous loading, a number of parallel micro-cracks connect with each other, and finally form a macroscopic shear failure surface through the annular surface of the sample. Therefore,

the angle between the macroscopic shear failure plane and the horizontal plane of the sample will gradually decrease with the increase of confining pressure (Fig. 14). There is an obvious linear relationship between the macroscopic failure angle γ and the confining pressure (goodness of fit $R^2=0.966$).

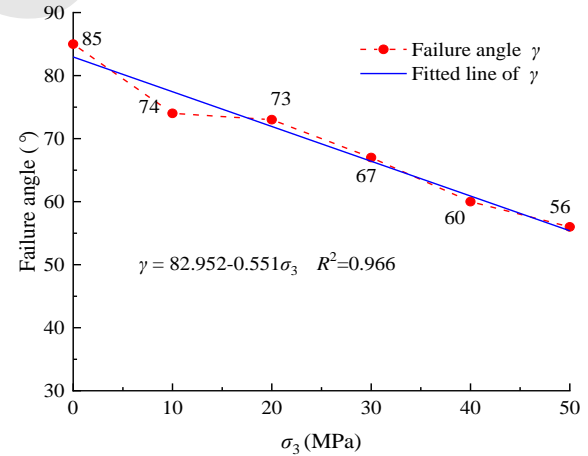


Fig. 14 Variation of the angle between the main failure plane and the horizontal plane with confining pressure

The macroscopic failure of the sample is the result of the convergence of cracks. Hence, the propagation direction of the cracks in the sample also linearly decreases with the increase of the confining pressure. In addition, the failure characteristics of

samples under triaxial compression of $\sigma_3=50$ MPa are different from those under $\sigma_3=30$ MPa, showing obvious shear plane damage (Fig. 13). This is because the direction of deviatoric stress on the sample changes with the increase of confining pressure. The composite action of high confining pressure and axial stress leads to increasing friction between the macroscopic shear planes of the samples, so that the samples with high confining pressure show more severe failure characteristics.

5 Conclusions

A quantitative analysis model was established to represent the initial proportion of micro-cracks in rock. Then, the range of the stress-strain curve was determined for accurate analysis of the initial micro-cracks. This model was verified against the triaxial experimental data. Finally, the evolution of cracks in the loaded samples was analyzed using CT scan images. From these investigations, we drew the following conclusions:

1. Each parameter in the quantitative analysis model for the initial proportion of micro-cracks in rock has a definite physical meaning. The model can accurately characterize the relationship between the overall macroscopic deformation and the deviatoric stress in both the compaction stage and linear elastic stage under triaxial compression.
2. The elastic modulus of the matrix first increases and then tends to be stable with increasing confining pressure, while that of micro-cracks increases exponentially. The sensitivity ranges of the sample matrix elastic modulus and micro-cracks to confining pressure were 0-30 MPa and 30-50 MPa, respectively.
3. The porosity and Poisson's ratio decreased according to an exponential function, and the decrement of porosity and Poisson's ratio in the σ_3 range of 0-10 MPa together accounted for 75% of the corresponding total decrement when σ_3 increased from 0 to 50 MPa. The increase of the initial proportion of micro-cracks increases the non-uniform deformation of the sample.
4. Failure results from the propagation process of micro-cracks. The number of cracks is highest and the tensile failure characteristics most obvious in uniaxial compression samples. Shear failure was obvious under triaxial compression. With increasing confining

pressure, the failure angle linearly decreased and the direction of propagation of the internal cracks (corresponding to different expansion modes) also showed a linear decrease.

Acknowledgments

We are grateful for financial support from the National Natural Science Foundation of China (12272119, U1965101).

Author contributions

Zhiliang WANG: Conceptualization, Data processing, Writing – review & editing, Supervision, Funding acquisition. Songyu LI: Conceptualization, Data processing, Formal analysis, Writing – original draft, Writing – review & editing. Jianguo WANG: Methodology, Writing – review & editing. Ao LI: Investigation, Visualization. Weixiang WANG: Writing – review & editing. Chenchen FENG: Writing – review & editing. Jingjing FU: Writing – review & editing.

Conflict of interest

Zhiliang WANG, Songyu LI, Jianguo WANG, Ao LI, Weixiang WANG, Chenchen FENG and Jingjing FU declare that they have no conflict of interest.

References

- Bahrani N, Kaiser PK, 2017. Estimation of confined peak strength of crack-damaged rocks. *Rock Mechanics and Rock Engineering*, 50, 309-326.
<https://doi.org/10.1007/s00603-016-1110-1>
- Bieniawski ZT, 1967. Mechanism of brittle fracture of rock, Parts I, II and III. *International Journal of Rock Mechanics and Mining Sciences and Geomechanical Abstracts*, 4(4):395-430.
[https://doi.org/10.1016/0148-9062\(67\)90030-7](https://doi.org/10.1016/0148-9062(67)90030-7)
- Cai JC, Wei W, Hu XY, et al., 2017. Electrical conductivity models in saturated porous media: A review. *Earth Science Reviews*, 171:419-433.
<https://doi.org/10.1016/j.earscirev.2017.06.013>
- Cao P, Cao RH, Zhao YL, et al., 2016. Propagation-coalescence and rheologic fracture behavior of rock cracks. *The Chinese Journal of Nonferrous Metals*, 26(08):1737-1762 (in Chinese).
<https://doi.org/10.19476/j.ysxb.1004.0609.2016.08.017>
- Cao P, Liu TY, Pu C, et al., 2015. Crack propagation and coalescence of brittle rock-like specimens with pre-existing cracks in compression. *Engineering Geology*, 187, 113-121.
<https://doi.org/10.1016/j.enggeo.2014.12.010>
- Chang SH, Lee CI, 2004. Estimation of cracking and damage mechanisms in rock under triaxial compression by moment tensor analysis of acoustic emission. *International Journal of Rock Mechanics and Mining Sciences*, 41(7): 1069-1086.
<https://doi.org/10.1016/j.ijrmms.2004.04.006>
- Chen T, 2017. Study on the techniques of active prevention

- and controlling of rock burst based on controlled blasting. MD Thesis, Wuhan University, Hubei, China (in Chinese).
- Corkum AG, Martin CD, 2007. The mechanical behaviour of weak mudstone (Opalinus Clay) at low stresses. *International Journal of Rock Mechanics and Mining Sciences*, 44 (2), 196-209.
<https://doi.org/10.1016/j.ijrmms.2006.06.004>
- Daniel T, Michał N, Jacek T, 2023. Application of the 3D DEM in the modelling of fractures in pre-flawed marble specimens during uniaxial compression. *Engineering Fracture Mechanics*, 277: 108978.
<https://doi.org/10.1016/j.engfracmech.2022.108978>
- David EC, Brantut N, Schubnel A, et al., 2012. Sliding crack model for nonlinearity and hysteresis in the uniaxial stress-strain curve of rock. *International Journal of Rock Mechanics and Mining Sciences*, 52:9-17.
<https://doi.org/10.1016/j.ijrmms.2012.02.001>
- Dehestani A, Kazemi F, Abdi R, et al., 2022. Prediction of fracture toughness in fibre-reinforced concrete, mortar, and rocks using various machine learning techniques. *Engineering Fracture Mechanics*, 276: 108914.
<https://doi.org/10.1016/j.engfracmech.2022.108914>
- Eberhardt E, Stead D, Stimpson B, et al., 1998. Identifying crack initiation and propagation thresholds in brittle rock. *Canadian Geotechnical Journal*, 35(2): 222-233.
<https://doi.org/10.1139/cgj-35-2-222>
- Fairhurst C, Hudson JA, 1999. Draft ISRM suggested method for the complete stress-strain curve for intact rock in uniaxial compression. *International Journal of Rock Mechanics and Mining Sciences*, 36(3):279-289.
[https://doi.org/10.1016/S0148-9062\(99\)00006-6](https://doi.org/10.1016/S0148-9062(99)00006-6)
- Freed AD, 1995. Natural strain. *Journal of Engineering Materials and Technology*, 117: 379-85.
<https://doi.org/10.1115/1.2804729>
- Johnson PA, Rasolofosaon PNJ, 1996. Nonlinear elasticity and stress-induced anisotropy in rock. *Journal of Geophysical Research: Solid Earth*, 101:3113-3124.
<https://doi.org/10.1029/95JB02880>
- Li HQ, Wong LNY, 2012. Influence of flaw inclination angle and loading condition on crack initiation and propagation. *International Journal of Solids and Structures*, 49(18): 2482-2499.
<https://doi.org/10.1016/j.ijsolstr.2012.05.012>
- Li SY, Wang ZL, Wang JG, et al., 2023. Analysis on mechanical behavior and progressive failure of deep-buried marble based on complete stress-strain curves. *Bulletin of Engineering Geology and the Environment*, 82, 133.
<https://doi.org/10.1007/s10064-023-03123-5>
- Li TC, Lyu, LX, Zhang SL, et al., 2015. Development and application of a statistical constitutive model of damaged rock affected by the load-bearing capacity of damaged elements. *Journal of Zhejiang University-SCIENCE A (Applied Physics & Engineering)*, 16(8):644-655.
<https://doi.org/10.1631/jzus.A1500034>
- Li XB, Gong FQ, Tao M, et al., 2017a. Failure mechanism and coupled static-dynamic loading theory in deep hard rock mining: A review. *Journal of Rock Mechanics and Geotechnical Engineering*, 9(04): 767-782.
<https://doi.org/10.1016/j.jrmge.2017.04.004>
- Li XZ, Qi CZ, Shao ZS, et al., 2018. Static shear fracture influenced by historic stresses path and crack geometries in brittle solids. *Theoretical and Applied Fracture Mechanics*, 96:64-71.
<https://doi.org/10.1016/j.tafmec.2018.04.002>
- Li YW, Jia D, Rui ZH, et al., 2017b. Evaluation method of rock brittleness based on statistical constitutive relations for rock damage. *Journal of Petroleum Science and Engineering*, 153:123-132.
<https://doi.org/10.1016/j.petrol.2017.03.041>
- Liu N, Zhang CS, Shan ZG, et al., 2019. Deep buried large and long tunnel supporting design and engineering practice under the risk of rock burst. *Chinese Journal of Rock Mechanics and Engineering*, 38(S1):2934-43 (in Chinese).
<https://doi.org/10.13722/j.cnki.jrme.2018.1086>
- Liu Y, Dai F, 2021. A review of experimental and theoretical research on the deformation and failure behavior of rocks subjected to cyclic loading. *Journal of Rock Mechanics and Geotechnical Engineering*, 13(05): 1203-1230.
<https://doi.org/10.1016/j.jrmge.2021.03.012>
- Martin CD, 1997. Seventeenth Canadian geotechnical colloquium: The effect of cohesion loss and stress path on brittle rock strength. *Canadian Geotechnical Journal*, 34(5):698-725.
<https://doi.org/10.1139/cgj-34-5-698>
- Mavko GM, Nur A, 1978. The effect of nonelliptical cracks on the compressibility of rocks. *Journal of Geophysical Research: Solid Earth*, 83:4459-4468.
<https://doi.org/10.1029/JB083iB09p04459>
- Morgan SP, Johnson CA, Einstein HH, 2013. Cracking processes in Barre granite: fracture process zones and crack coalescence. *International Journal of Fracture*, 180 (2), 177-204.
<https://doi.org/10.1007/s10704-013-9810-y>
- Nur A, 1971. Effects of stress on velocity anisotropy in rocks with cracks. *Journal of Geophysical Research: Solid Earth*, 76:2022-2034.
<https://doi.org/10.1029/JB076i008p02022>
- Pakzad SS, Roshan N, Ghalehnovi M, 2023. Comparison of various machine learning algorithms used for compressive strength prediction of steel fiber-reinforced concrete. *Scientific Reports*, 13, 3646.
<https://doi.org/10.1038/s41598-023-30606-y>
- Peng J, Rong G, Zhou CB, et al., 2016. A study of crack closure effect of rocks and its quantitative model. *Rock and Soil Mechanics*, 37(01):126-132 (in Chinese).
<https://doi.org/10.16285/j.rsm.2016.01.015>
- Rosengren KJ, Jaeger JC, 1968. The mechanical properties of an interlocked low-porosity aggregate. *Géotechnique*, 18(3): 317-326.
<https://doi.org/10.1680/geot.1968.18.3.317>
- Saadat M, Taheri, A, 2019. Modelling micro-cracking behaviour of pre-cracked granite using grain-based distinct

- element model. *Rock Mechanics and Rock Engineering*, 52, 4669-4692.
<https://doi.org/10.1007/s00603-019-01862-0>
- Shreedharan S, Kulatilake P, 2016. Discontinuum-equivalent continuum analysis of the stability of tunnels in a deep coal mine using the distinct element method. *Rock Mechanics and Rock Engineering*, 49:1903-1922.
<https://doi.org/10.1007/s00603-015-0885-9>
- Taheri A, Zhang Y, Munoz H, 2020. Performance of rock crack stress thresholds determination criteria and investigating strength and confining pressure effects. *Construction and Building Materials*, 243:118263.
<https://doi.org/10.1016/j.conbuildmat.2020.118263>
- Tang Y, Okubo S, Xu J, et al., 2019. Progressive failure behaviors and crack evolution of rocks under triaxial compression by 3D digital image correlation. *Engineering Geology*, 249:172-85.
<https://doi.org/10.1016/j.enggeo.2018.12.026>
- Wang ZL, Li SY, Wang JG, et al., 2022. Mechanical behavior, mesoscopic properties and energy evolution of deeply buried marble during triaxial loading. *International Journal of Damage Mechanics*, 31(10):1592-1612.
<https://doi.org/10.1177/10567895221107707>
- Wu ZJ, Fan LF, Liu QS, et al., 2017. Micro-mechanical modeling of the macro-mechanical response and fracture behavior of rock using the numerical manifold method. *Engineering Geology*, 225, 49-60.
<https://doi.org/10.1016/j.enggeo.2016.08.018>
- Xie HP, 2019. Research review of the state key research development program of China: Deep rock mechanics and mining theory. *Journal of China Coal Society*, 44(5): 1283-1305 (in Chinese).
<https://doi.org/10.13225/j.cnki.jccs.2019.6038>
- Xie SJ, Han ZY, Lin H, 2022. A quantitative model considering crack closure effect of rock materials. *International Journal of Solids and Structures*, 251:11758.
<https://doi.org/10.1016/j.ijsolstr.2022.111758>
- Xu P, Peng P, Wei RH, et al., 2022. Model test of the mechanism underpinning water-and-mud inrush disasters during tunnel excavation in sandstone and slate interbedded Presinian strata. *Journal of Zhejiang University-SCIENCE A (Applied Physics & Engineering)* 23(11), 882-899.
<https://doi.org/10.1631/jzus.A2200134>
- Zhang C, Chen QN, Yang QJ, et al., 2020. Whole process simulation method of brittle rocks deformation and failure considering initial voids closure and its influence. *Journal of China Coal Society*, 45(03):1044-1052 (in Chinese).
<https://doi.org/10.13225/j.cnki.jccs.2019.0221>
- Zhang PS, Xu DQ, Zhang R, et al., 2022. Experimental study on seepage and mechanical properties of sandstone under different confining pressures and cyclic loads. *Chinese Journal of Rock Mechanics and Engineering*, 41(12):2432-2450 (in Chinese).
<https://doi.org/10.13722/j.cnki.jrme.2022.0241>
- Zhang QB, Zhao J, 2014. A Review of Dynamic Experimental Techniques and Mechanical Behaviour of Rock Materials. *Rock Mechanics and Rock Engineering*, 47:1411-1478.
<https://doi.org/10.1007/s00603-013-0463-y>
- Zhang Y, Li BB, Xu Jiang, et al., 2021. Study on triaxial compression damage evolution characteristics of coal based on energy dissipation. *Chinese Journal of Rock Mechanics and Engineering*, 40(08):1614-1627 (in Chinese).
<https://doi.org/10.13722/j.cnki.jrme.2020.1133>
- Zhao Y, Liu HH, 2012. An elastic stress - strain relationship for porous rock under anisotropic stress conditions. *Rock Mechanics and Rock Engineering*, 45(3):389-399.
<https://doi.org/10.1007/s00603-011-0193-y>
- Zhao YL, Wang YX, Wang WJ, et al., 2017. Modeling of non-linear rheological behavior of hard rock using triaxial rheological experiment. *International Journal of Rock Mechanics and Mining Sciences*, 93:66-75.
<https://doi.org/10.1016/j.ijrmms.2017.01.004>
- Zhou HW, Wang ZH, Ren WG, et al., 2019a. Acoustic emission based mechanical behaviors of Beishan granite under conventional triaxial compression and hydro-mechanical coupling tests. *International Journal of Rock Mechanics and Mining Sciences*, 123:104125.
<https://doi.org/10.1016/j.ijrmms.2019.104125>
- Zhou SW, Zhuang XY, Zhu HH, et al., 2018. Phase field modelling of crack propagation, branching and coalescence in rocks. *Theoretical and Applied Fracture Mechanics*, 96, 174-192.
<https://doi.org/10.1016/j.tafmec.2018.04.011>
- Zhou T, Zhu JB, Ju Y, et al., 2019b. Volumetric fracturing behavior of 3D printed artificial rocks containing single and double 3D internal flaws under static uniaxial compression. *Engineering Fracture Mechanics*, 205, 190-204.
<https://doi.org/10.1016/j.engfracmech.2018.11.030>
- Zhou XP, Cheng H, Feng YF, 2014. An experimental study of crack coalescence behaviour in rock-like materials containing multiple flaws under uniaxial compression. *Rock Mechanics and Rock Engineering*, 47, 1961-1986.
<https://doi.org/10.1007/s00603-013-0511-7>
- Zuo JP, Chen Y, Liu XL, 2019. Crack evolution behavior of rocks under confining pressures and its propagation model before peak stress. *Journal of Central South University*, 26(11): 3045-3056.
<https://doi.org/10.1007/s11771-019-4235-z>

中文概要

题目：大理岩三轴压缩初始微裂纹演化机理及定量表征

作者：王志亮¹，李松玉¹，王建国²，李傲¹，王伟祥¹，封陈晨¹，傅晶晶¹

机构：¹合肥工业大学，土木与水利工程学院，中国合肥，

230009; ² 中国矿业大学, 力学与土木工程, 中国徐州, 221116

目的: 岩石宏观变形破坏演化特征受其内部初始微裂纹的影响, 但在理论计算、数值模拟和力学实验中这部分影响往往被忽略。本文提出了一个定量分析模型来研究初始微裂纹对岩石变形破坏演化过程的影响。

创新点: 1. 建立了初始微裂纹占比定量分析的理论模型;
2. 揭示了围压对大理岩模型参数演化的影响。

方法: 1. 通过理论推导, 建立了一种能进行岩石初始微裂纹占比定量分析的理论模型, 并基于三轴压缩试样的应力分解改进了该模型的表达式(公式(13)和(14)); 2. 通过三轴压缩试验, 确定了岩石初始裂隙精确分析的拟合区间, 并分析了围压对大理岩试样模型参数演化的影响(图 6-8); 3. 结合微 CT 扫描技术, 对受载岩样的裂隙演化特征进行讨论与分析(图 12 和 13)。

结论: 1. 所发展的岩石初始微裂纹占比定量分析模型参数物理意义明确、确定方便; 2. 随围压的增加, 试样孔隙度和泊松比均指数函数递减, 基质部分弹性模量先增大后趋于稳定, 微裂纹弹性模量指数增长; 3. 试样破坏是其内部微裂纹的扩展的结果, 宏观破坏角随着围压的增大呈线性减小。

关键词: 岩石材料; 初始微裂纹; 三轴压缩; 本构关系; 裂纹演化